Proceedings of the IASS 2024 Symposium
Redefining the Art of Structural Design
August 26-30, 2024, Zurich, Switzerland
Philippe Block, Giulia Boller, Catherine DeWolf,
Jacqueline Pauli, Walter Kaufmann (eds.)

Isogeometric form-finding of membrane shells based on single-objective optimized Airy stress function

Claudia CHIANESE*, Francesco MARMO[a], Luciano ROSATI[b]

* Department of Structures for Engineering and Architecture
Via Claudio 21, 80125, Naples, Italy
claudia.chianese@unina.it

Abstract

Membrane shells identify expressive architectural solutions for resistant but lightweight structures of appealing aesthetic taste thanks to their ability to span wide areas with careful usage of material in the absence of flexural and torsional internal actions. The design philosophy, seeking the shell shape endowed with such moment-free quality, is known as form finding. To circumvent the indeterminacy of the related boundary-value problem, the state of stress is conventionally prescribed by assigning the Airy potential function so that the resulting shell form can be statically computed. Despite their practicality, traditional algorithms subtly restrict form finding to shells with rather simple planar configurations, whereby a feasible potential field is susceptible of an analytical description. In any case, auxiliary functional requirements cannot be properly accounted for during the process. In this study, we present a two-step numerical form-finding strategy suited to assist the designer in the selection of a proper potential field satisfying standard static and user-defined functional constraints. Use of isogeometric analysis ensures high-precision modelling of the form-found geometry, making the approach adapt to shells of complex planar forms. Two examples show the effectiveness of the procedure, where the influence of kinematic boundary conditions on the form-found geometry is also highlighted.

Keywords: form finding, isogeometric analysis, membrane shells, concrete spatial structures, Pucher's theory, Airy stress function, single-objective optimization.

1. Introduction

Membrane shells are favored in contemporary civil engineering owing to a bearing capacity relying on a system of purely in-plane internal actions. The intrinsic absence of flexural and torsional moments identifies this kind of structures as a convenient architectural solution to span wide areas with careful usage of material without resorting to obstructive supporting pillars. The design philosophy, seeking the shell shapes endowed with such moment-free property, is termed form finding [1].
To tackle the indeterminacy of the related boundary-value problem, the majority of existing form-finding algorithms assign the stress field as an input in the form of a suitable Airy stress function, then solve for the corresponding shell equilibrium configuration. In spite of its undoubted practicality, this approach subtly limits the process to relatively simple shell forms. For instance, the prescription of a feasible Airy stress function, complying with static boundary conditions in force, is not trivial when shells with intricate planar footprints are addressed [2, 3]. Moreover, the manual adjustment of the user-prescribed potential field tends to be generally far from intuitive in the presence of auxiliary functional requirements setting the shell height or curvature in specific regions of the membrane, due to its abstract nature [4].
In this paper, a numerical form-finding strategy, based on isogeometric analysis (IgA) [5], is presented to determine the configuration of shells, made of a unilateral material, having a specified planar foot-

print. With predefined external loads, the procedure first delivers an optimized Airy stress function as a solution of a nonlinear programming routine aimed at minimizing the thrusts conveyed to the supports of the structure while ensuring no-traction working stresses under relevant static boundary conditions. The corresponding shell form is subsequently obtained compatibly with imposed kinematic constraints. In contrast to the manual prescription of the Airy stress function, the proposed strategy results to be a versatile tool to assist the designer in determining a locally optimal geometry accounting for usual static as well as user-defined functional constraints.
The paper is organized as follows. Section 2 briefly introduces the reader to the mathematical formulation of the membrane shell boundary-value problem. The isogeometric discretization model and the proposed optimization routine are in turn detailed in Section 3 and Section 4. Results are then discussed in Section 5. Eventually, conclusions are drawn in Section 6.

2. The membrane shell boundary-value problem

Among various membrane formulations available in the literature [6], Pucher's theory [7] can be regarded as the most adapt to deal with form-finding problems given its applicability to funicular shells of general shape. Within that model, the equilibrium of a shell infinitesimal element, acted upon by distributed loads and internal actions, is governed by the following equation:

$$\nabla^2\Phi\nabla^2 f - \nabla(\nabla\Phi)\cdot\nabla(\nabla f) = (\mathbf{q}^h\cdot\nabla f) + \mathbf{h}\cdot(\nabla\circ\nabla f) - q_z \tag{1}$$

where ∇^2 is the Laplacian operator, $\boldsymbol{\nabla} = [\partial/\partial x, \partial/\partial y]^T$, $\mathbf{h} = [\int q_x\,dx, \int q_y\,dy]^T$, $\mathbf{q} = [q_x, q_y, q_z] \equiv [\mathbf{q}^h, q_z]$ the external force per unit projected area, f the height of the shell mid-surface S, and Φ the Airy stress function associated with the projected membrane stress components, i.e.:

$$N_x = \Phi_{,yy} - \int q_x\,dx \qquad N_y = \Phi_{,xx} - \int q_y\,dy \qquad N_{xy} = -\Phi_{,xy} \tag{2}$$

Complemented with relevant boundary conditions, Eq.(1) encloses the strong form of the membrane shell boundary-value problem.
Let $\mathcal{F} = \{f(x,y)|f(x,y) = \bar{f}(x,y)\ \forall(x,y)\in\Gamma_c\}$ be the functional space where to seek the shape of $\mathcal{S}$ fulfilling geometric boundary conditions on the shell restrained boundary Γ_c. Again, be $\mathcal{G} = \{g(x,y)|g(x,y) = 0\ \forall(x,y)\in\Gamma_c\}$ the set of arbitrary weight functions of f vanishing on Γ_c. Applying the chain rule on the terms involving the second derivatives of f and eliminating similar addends, Eq.(1), pre-multiplied by g on both sides, can be written as:

$$\begin{aligned} div\{\nabla^2\Phi\nabla f - \nabla f^T\nabla(\nabla\Phi) - \mathbf{h}\circ\nabla f\}g + [\nabla f^T\nabla(\nabla\Phi)]\cdot\nabla g - \\ + \nabla^2\Phi(\nabla f\cdot\nabla g) + (\mathbf{h}\circ\nabla f)\cdot\nabla g = -q_z g \quad \forall g\in\mathcal{G} \end{aligned} \tag{3}$$

Integration of Eq.(3) over the shell projected domain Ω, combined with the divergence theorem, eventually delivers the weak form of the problem at hand:

$$\begin{aligned} \int_\Omega \Big[\nabla^2\Phi(\nabla f\cdot\nabla g) - [\nabla f^T\nabla(\nabla\Phi)]\cdot\nabla g - (\mathbf{h}\circ\nabla f)\cdot\nabla g\Big]\,d\Omega = \\ \int_{\Gamma_f} g\Big[\nabla^2\Phi\nabla f - \nabla f^T\nabla(\nabla\Phi) - (\mathbf{h}\circ\nabla f)\Big]\cdot\hat{\mathbf{n}}\,ds + \int_\Omega q_z g\,d\Omega \quad \forall g\in\mathcal{G} \end{aligned} \tag{4}$$

having denoted with Γ_f the free boundary of the shell and $\hat{\mathbf{n}}$ its normal unit vector.

3. The isogeometric computational model

An exact solution to the weak form can be sought only in exceptionally simple cases. In this study, the isogeometric computational model is employed to approximately find the shell mid-surface elevation $f(x, y)$ as a solution of a linear algebraic system, obtained upon discretization of Eq.(4). Ergo, the shell domain Ω is modelled by N^e elements of a single B-Spline surface patch, confined within pairs of knot spans along the parametric directions ξ and η, i.e. $\Omega^e = [\xi_i, \xi_{i+1}] \times [\eta_j, \eta_{j+1}]$. Thus:

$$\sum_{e=1}^{N^e} \int_{\Omega^e} \nabla^2\Phi^e(\nabla\, f^e \cdot \nabla\, g^e) - [(\nabla\, f^e)^T \nabla(\nabla\, \Phi^e)] \cdot \nabla\, g^e - (\mathbf{h}^e \circ \nabla\, f^e) \cdot \nabla\, g^e \, d\Omega^e = \sum_{e=1}^{N^e} \int_{\Omega^e} q_z^e g^e \, d\Omega^e \quad (5)$$

Note that the integral on Γ_f has been left out in the above expression because null as long as the prescribed stress field complies with the static conditions (13) imposed on the shell free frontier.
Within the IgA framework, the distribution of the relevant fields f, g and Φ within an element is evaluated as a linear combination of n_{cp}^e values at control points via the corresponding B-Spline basis functions. Thus,

$$f^e(\xi,\eta) = S_k^e Z_k^e \Leftrightarrow f^e(\xi,\eta) = \left[R_1(\xi,\eta)...R_{n_{cp}^e}(\xi,\eta)\right]\left[f_1...f_{n_{cp}^e}\right]^T$$

$$f_{,j}^e(\xi,\eta) = B_{jk}^e Z_k^e \Leftrightarrow \begin{bmatrix} f_{,x}(\xi,\eta) \\ f_{,y}(\xi,\eta) \end{bmatrix} = \begin{bmatrix} R_{1,x}(\xi,\eta)...R_{n_{cp}^e,x}(\xi,\eta) \\ R_{1,y}(\xi,\eta)...R_{n_{cp}^e,y}(\xi,\eta) \end{bmatrix}\left[f_1...f_{n_{cp}^e}\right]^T$$

The approximation scheme for g and Φ holds in a similar fashion when the corresponding vectors of the field values at control points are denoted as $\mathbf{W}^e$ and $\mathbf{A}^e$, respectively.
Likewise, $\nabla(\nabla\Phi^e)$ is computed via a three-dimensional tensor, containing the second-order derivatives of the basis functions, times a vector of Φ-values at control points: $\Phi_{,ij}^e(\xi,\eta) = C_{ijm}^e(\xi,\eta)A_m^e$, where $i, j = \{x, y\}$ and $m = 1, .., n_{cp}^e$. Therefore:

$$\nabla^2\Phi(\xi,\eta) = L_p^e(\xi,\eta)\; P_p^e = \\ = [C_{111}(\xi,\eta)\; ...\; C_{11n_{cp}^e}(\xi,\eta)|C_{221}(\xi,\eta)\; ...\; C_{22n_{cp}^e}(\xi,\eta)][\Phi_1\; ...\; \Phi_{n_{cp}^e}|\Phi_1\; ...\; \Phi_{n_{cp}^e}]^T$$

By virtue of the above discretization scheme, Eq.(5) becomes:

$$\sum_{e=1}^{N^e} \left[\int_{\Omega^e} (\mathbf{L}^e \cdot \mathbf{P}^e)(\mathcal{B}^{e^T}\mathcal{B}^e) - \mathcal{B}^{e^T}(\mathbb{C}^e\mathbf{A}^e)\mathcal{B}^e - \mathcal{B}^{e^T}(\mathbf{h}^e \circ \mathcal{B}^e) d\Omega^e \right] \mathbf{Z}^e \cdot \mathbf{W}^e = \\ = \sum_{e=1}^{N^e} \left[\int_{\Omega^e} q_z^e \mathbf{S}^e d\Omega^e \right] \cdot \mathbf{W}^e \quad (6)$$

For clarity of reading, scalars, vectors, 2^{nd}- and 3^{rd}-order tensors have been denoted as italic, bold, calligraphic bold and blackboard bold font styles, respectively.
Because a B-Spline patch corresponds to a parallelepiped in the parameter space, Gauss-Legendre quadrature is a natural candidate for numerical integrations in Eq.(6). Distinctly from the conventional finite-element method, an additional mapping from the physical to the parametric domain is required during the integration process: $\hat{\phi} : \Omega^e \rightarrow \hat{\Omega}^e$. Isogeometric elements are then mapped to a regularly shaped bi-unit reference one: $\tilde{\phi} : \hat{\Omega}^e \rightarrow \tilde{\Omega}^e$.

The inverse mapping $\tilde{\phi}^{-1}$ to an element $\hat{\Omega}^e = [\xi_i, \xi_{i+1}] \otimes [\eta_j, \eta_{j+1}]$ is regulated by:

$$\xi = \frac{1}{2}[(\xi_{i+1} - \xi_i)\tilde{\xi} + (\xi_{i+1} + \xi_i)] \qquad \eta = \frac{1}{2}[(\eta_{j+1} - \eta_j)\tilde{\eta} + (\eta_{j+1} + \eta_j)]$$

where $\tilde{\xi}$ and $\tilde{\eta}$ denote the coordinates of Gaussian points in the reference element.
Thus, a generic integrand $f(x, y)$ can be numerically integrated over an element according to:

$$\int_{\Omega^e} f(x, y)\, d\Omega^e = \sum_{q=1}^{n_{gp}} f(\tilde{\xi}_q, \tilde{\eta}_q) w_{gp_q} |\mathcal{J}_{\hat{\phi}}| |J_{\tilde{\phi}}|$$

where n_{gp} and w_{gp_q} are the number of Gaussian points and associated weights while the Jacobian matrices associated with the two mappings are defined as:

$$\mathcal{J}_{\hat{\phi}} = \begin{bmatrix} \frac{\partial x}{\partial \hat{\xi}} & \frac{\partial x}{\partial \hat{\eta}} \\ \frac{\partial y}{\partial \hat{\xi}} & \frac{\partial y}{\partial \hat{\eta}} \end{bmatrix} \qquad J_{\tilde{\phi}} = \frac{\partial \hat{\xi}}{\partial \tilde{\xi}} \frac{\partial \hat{\eta}}{\partial \tilde{\eta}}$$

Through element assemblage, Eq.(6) can be arranged into a customary global format:

$$(\mathcal{K}\mathbf{Z}) \cdot \mathbf{W} = \mathbf{Q} \cdot \mathbf{W} \tag{7}$$

where $\mathcal{K}$ takes the meaning of shell stiffness matrix.
Given the arbitrariness of $\mathbf{W}$, Eq.(7) further simplifies to:

$$\mathcal{K}\mathbf{Z} = \mathbf{F} + \mathbf{Q} \tag{8}$$

being $\mathbf{F}$ the vector of control point residuals, which are nonzero only at constrained control points, thereby equal to the reactions exerted by the supports.
To solve the above algebraic system for the unknown components of $\mathbf{Z}$ and $\mathbf{F}$, it is recommended to separate both vectors $\mathbf{Z}$ and $\mathbf{Q}$ into two sub-vectors pertaining to the degrees of freedom where the shell height is prescribed [resp., unknown] (subscript P) [resp., (subscript U)]. Thus:

$$\begin{bmatrix} \mathcal{K}_{PP} & \mathcal{K}_{PU} \\ \mathcal{K}_{UP} & \mathcal{K}_{UU} \end{bmatrix} \begin{bmatrix} \mathbf{Z}_P \\ \mathbf{Z}_U \end{bmatrix} = \begin{bmatrix} \mathbf{F}_P \\ \mathbf{F}_U \end{bmatrix} + \begin{bmatrix} \mathbf{Q}_P \\ \mathbf{Q}_U \end{bmatrix} \tag{9}$$

Accounting for the imposed position of restrained control points, the form-found geometry can be eventually constructed by computing the elevation of free control points according to:

$$\mathbf{Z}_U = \mathcal{K}_{UU}^{-1}[\mathbf{F}_U + \mathbf{Q}_U - \mathcal{K}_{UP}\mathbf{Z}_P] \tag{10}$$

Then, the reaction forces exerted by the supports at restrained control points result from:

$$\mathbf{F}_P = \mathcal{K}_{PP}\mathbf{Z}_P + \mathcal{K}_{PU}\mathbf{Z}_U - \mathbf{Q}_P \tag{11}$$

4. Optimization of the Airy stress function

Use of Eqs. (10)-(11) requires that a feasible Airy stress function is first provided in order to compute the components of $\mathcal{K}$. In this section, a nonlinear programming routine is set up to automatically determine an optimized potential field taking into account static as well as functional constraints. Within the application purposes of the present study, the shell structure is assumed to be made of a unilateral material incapable of resisting tensile stresses. Accordingly, without any loss of generality, the proposed

optimization procedure is finalized to minimize the thrusts conveyed to the supports of the structure, a condition intended thereby as a functional requirement herein.
Hence, denoting by $\mathcal{N}$ the projected membrane stress tensor, the no-traction assumption requires $\mathcal{N}$ to be negative semi-definite throughout the shell domain, i.e. $(\mathcal{N}\hat{\mathbf{v}})\hat{\mathbf{v}} \leq 0, \forall \hat{\mathbf{v}} \in \Omega$, that is:

$$\begin{aligned} tr\mathcal{N} &= N_x + N_y = (\Phi_{,yy} - h_x) + (\Phi_{,xx} - h_y) \leq 0 \\ det\mathcal{N} &= N_x N_y - N_{xy}^2 = (\Phi_{,yy} - h_x)(\Phi_{,xx} - h_y) - \Phi_{,xy}^2 \geq 0 \end{aligned} \tag{12}$$

Fulfillment of the static condition of null membrane stresses at control points, located on any free edge of the shell, is also demanded:

$$\mathcal{N}\hat{\mathbf{n}} = 0 \quad \text{on} \quad \Gamma_f \quad \rightarrow \quad \begin{cases} (\Phi_{,yy} - h_x)\hat{n}_x - \Phi_{,xy}\hat{n}_y = 0 \\ \Phi_{,yx}\hat{n}_x - (\Phi_{,xx} - h_y)\hat{n}_y = 0 \end{cases} \tag{13}$$

Being

$$T = |(\mathcal{N}\hat{\mathbf{n}})\hat{\mathbf{n}}| = |(\Phi_{,yy} - h_x)\hat{n}_x^2 - 2\Phi_{,xy}\hat{n}_x\hat{n}_y + (\Phi_{,xx} - h_y)\hat{n}_y^2|$$

the magnitude of the thrust conveyed to the support at the generic control point of the constrained boundary Γ_c, a suitable Φ field is sought via the MatLab© optimization routine `fmincon` by minimizing the objective function:

$$\text{obj} = |T_{max} - T_{threshold}| \tag{14}$$

subject to the nonlinear constraints in Eqs. (12)-(13). Convergence of the proposed numerical procedure ensures that the corresponding distribution of membrane stresses is such that reaction forces, acting on the supports of the structure, are within the user-defined upper limit value $T_{threshold}$.
A scheme of the workflow involved by the present form-finding procedure is available in Fig. 1, where its step-wise arrangement is also highlighted.

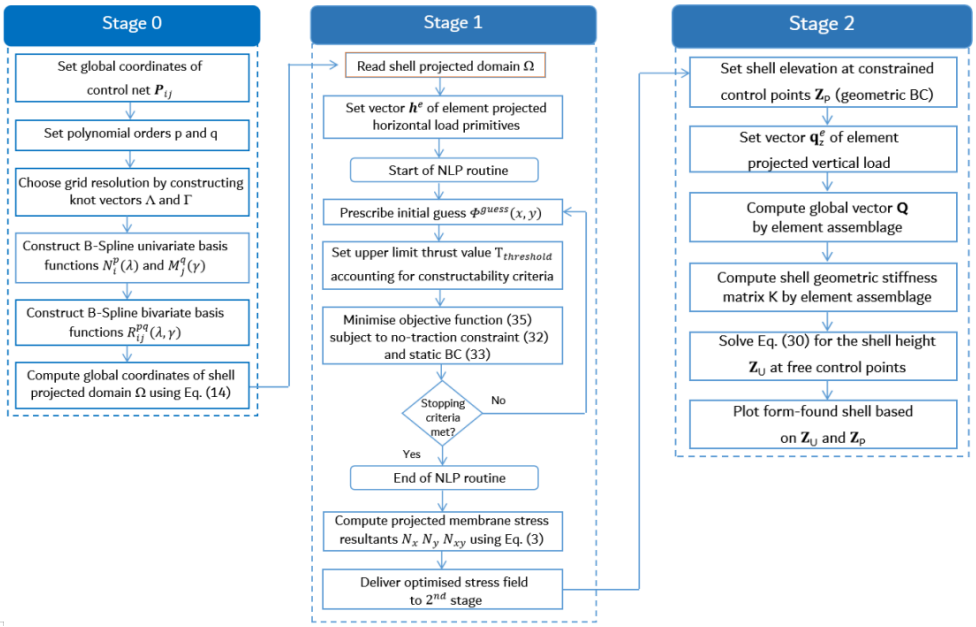

Figure 1: Schematic of present form-finding procedure.

5. Results

Two cases of fully compressed shells are illustrated in this section. As detailed in Fig. 1, the procedure starts from a flat surface having a planar footprint coincident with the target one. In both cases, the planar domain is a 4-meter-long square supported in cornered regions. Different extensions of the constrained bases are investigated to highlight their influence on the final geometry. In both examples, the initial geometry is discretised by 64 bicubic B-Spline elements and 225 control points having support on non-uniform open knot vectors $\Xi = H$ = [0, 0, 0, 0, 0.12, 0.12, 0.12, 0.15, 0.28, 0.50, 0.72, 0.84, 0.87, 0.87, 0.87, 1, 1, 1, 1]. Because of the non-interpolatory nature of spline technology, this choice allows to discretize the computational domain by equally-sized elements while imposing knots of triple multiplicity at the inner sides of the restrained cornered regions, where the form-found shape has to possess the heights specified by the kinematic boundary conditions. In both examples, the membrane is acted upon by a uniform projected vertical load q_z of 2 kN/m^2, exemplifying its weight.

5.1. Shell supported at cornered regions on its frontier

The shell is supported at cornered regions on its frontier while all edges are free. According to Eqs. (12)-(13), the Φ-distribution must be sought among the concave functions having no curvature variations along each edge of the shell. A parabolic velaroidal surface was then tentatively prescribed as an initial guess:

$$\Phi^{guess}(x,y) = -1100 \left(\frac{x^2}{a^2} + \frac{y^2}{b^2} - \frac{x^2 y^2}{a^2 b^2} \right) \quad \text{[Nm]} \qquad \forall (x,y) \in \Omega$$

where a and b are half-spans in the direction of the respective coordinate axes x and y while the multiplication factor of the term in brackets is the rise of the surface at its center.
On account of the non-convex format of the optimization problem, numerical convergence was attained by means of the robust Sequential Quadratic Programming (SQP) algorithm with $T_{threshold} = 2.47$ kN and relative constraint and step tolerances equal to $1E-06$ and $1E-10$, in turn. The optimized Airy stress function and corresponding principal projected membrane stresses are visualized in Fig. 2. The distribution of right stress eigenvectors is also reported in the same figure, where the absence of stresses across all free edges can be noticed according to Eq. (13). There, blue and red colours have been used to denote the directions associated with principal membrane stress resultants N_1 and N_2, in turn. Eventually, an isometry of the form-found geometry is depicted in the same figure, where the compliance with the geometric boundary conditions on the supported cornered regions can be also pointed out.

5.2. Shell supported at cornered regions of squared extension

In this second example, the extension of the cornered supports is enlarged to cover regions of squared footprint while leaving all edges free. Being the planar domain unchanged compared to the previous case, the optimization routine was again initiated again via a velaroidal guess:

$$\Phi^{guess}(x,y) = -2300 \left(\frac{x^2}{a^2} + \frac{y^2}{b^2} - \frac{x^2 y^2}{a^2 b^2} \right) \quad \text{[Nm]} \qquad \forall (x,y) \in \Omega$$

where a higher multiplication factor was adopted to achieve shell elevations not larger than 4 metres.
Fig. 3 displays the corresponding no-tensile locally optimal solution obtained for this case study. The settings used for the termination of the optimization routine are: $T_{threshold}$ = 3.91 kN, relative constraint tolerance = $1E-06$, relative step tolerance = $1E-10$. As in the previous case, the final distribution of the Airy stress function deviates considerably from the initial guess at the corners, where the alteration produced by the optimization solver in containing the magnitude of the edge constraint reactions can be

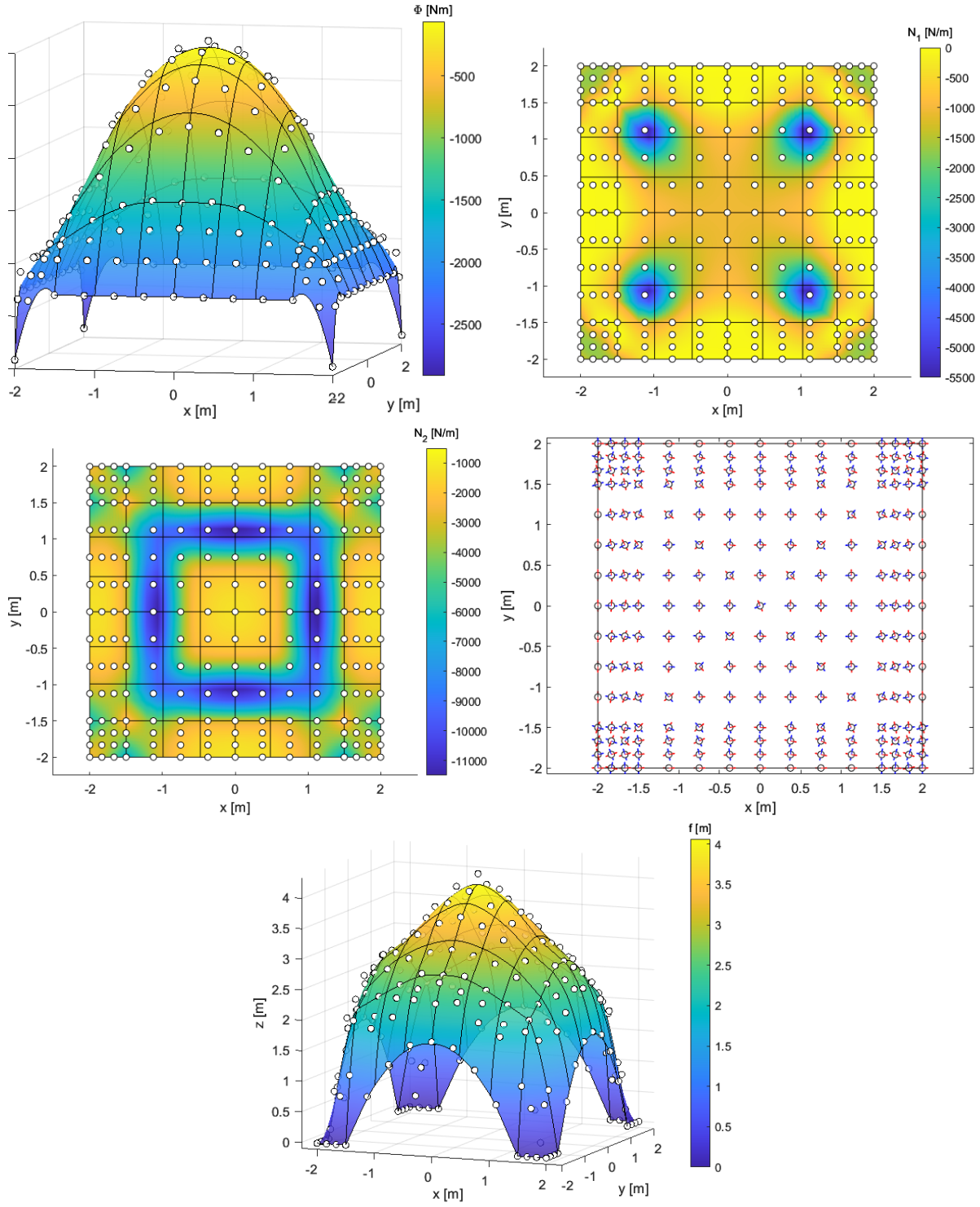

Figure 2: Optimized Airy stress function Φ (top left), projected principal membrane stress resultants (top right and middle left), right stress eigenvectors (middle right) and isometric view of form-found shell (bottom). Control points are denoted by white dots while element boundaries are depicted as black solid lines.

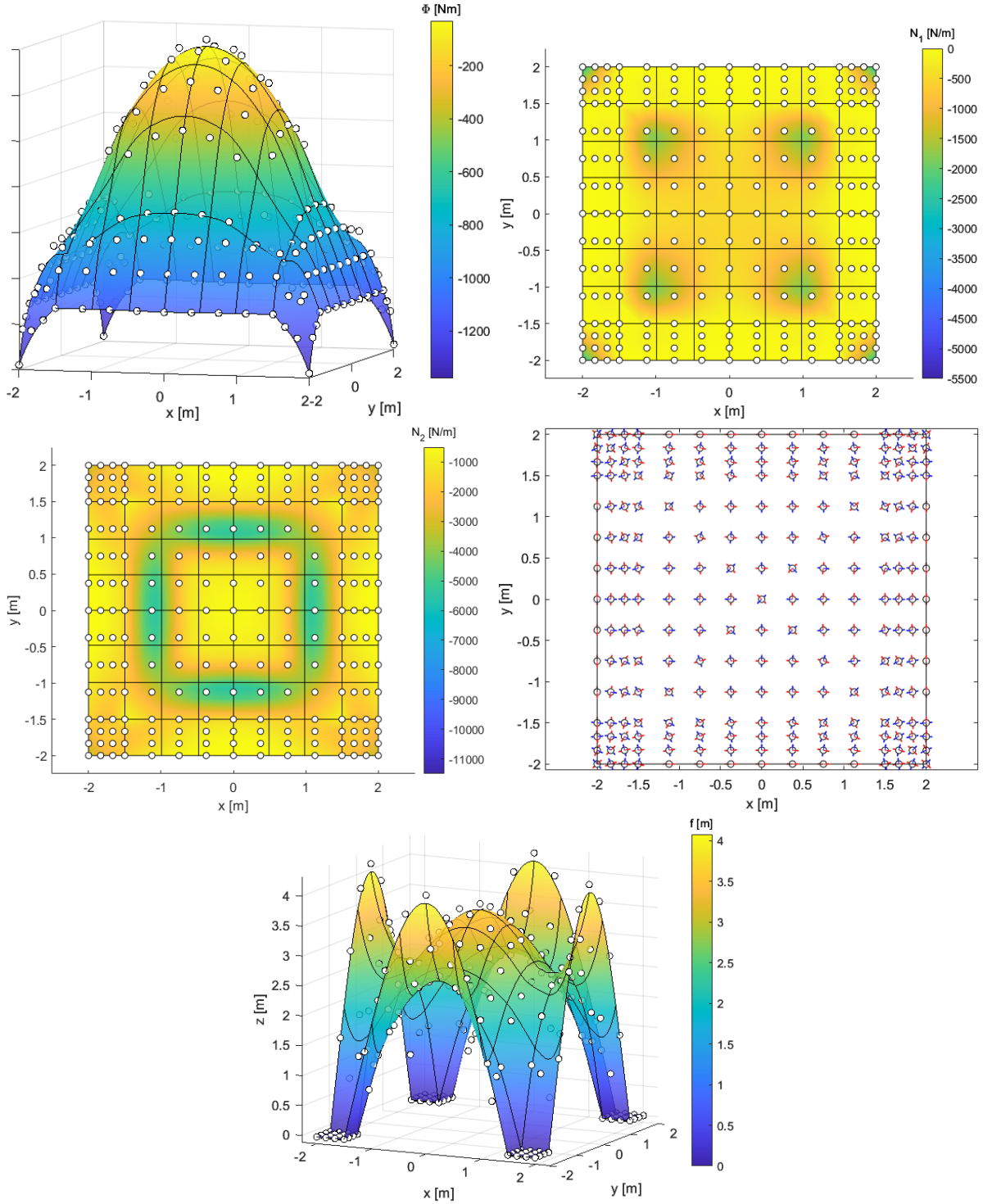

Figure 3: Airy stress function Φ (top left), projected principal membrane stress resultants (top right and middle left), right stress eigenvectors (middle right) and isometric view of form-found shell (bottom). Control points are denoted by white dots while element boundaries are depicted as black solid lines.

observed. It is remarked that the planar extension of the supports results to have a significant influence on the outcome of the overall procedure. In particular, a comparable sensitivity of the form-found geometry is evident on shell edges relative to the previous case.

6. Conclusions

A form-finding strategy, based on Pucher's theory, has been presented. The procedure determines the form of a shell of given planar footprint so as to balance applied loads in a state of purely in-plane stresses. Use of isogeometric analysis, as a numerical solving approach for the physical problem at hand, makes the algorithm applicable to shells of general free-form boundaries. In contrast with the standard analytical prescription of the Airy stress function, the integration of the proposed automatic optimization routine into the present form-finding procedure results to be a viable approach to guide the designer towards more functional architectural solutions.

Acknowledgements

This work was carried out within the "Modelling, Analysis and DEsign of MOrphing SHElls. MADEMOSHE" project - CUP E53D23003890006 - grant number 2022XFPZ5R – funded by the European Union – Next Generation EU, which is gratefully acknowledged by the authors.

References

[1] D. Veenendaal and P. Block, "An overview and comparison of structural form finding methods for general networks," *International Journal of Solids and Structures*, vol. 49, pp. 3741–3753, 2012.

[2] Y. Xia, A. Mantzaflaris, B. Jüttler, H. Pan, P. Hu, and W. Wang, "Design of self-supporting surfaces with isogeometric analysis," *Computer Methods in Applied Mechanics and Engineering*, vol. 353, pp. 328–347, 2019.

[3] F. Marmo and N. Vaiana, *Form finding of shell structures by using membrane theory*. Springer, 2021, pp. 213–237.

[4] F. Marmo *et al.*, "On the form of the musmeci's bridge over the basento river," *Engineering Structures*, vol. 191, pp. 658–673, 2019.

[5] J. A. Cottrell, T. J. Hughes, and B. Y., *Isogeometric analysis: Towards integration of CAD and FEA*. Wiley, 2009.

[6] W. Flügge, *Stresses in shells*. Springer, 2013.

[7] A. Pucher, "Über den spannungszustand in gekrümmten flächen," pp. 33–298, 1934.